Diamond & Related Materials 101 (2020) 107556

Contents lists available at ScienceDirect

Diamond & Related Materials

journal homepage: www.elsevier.com/locate/diamond

Crystalline transformation from ta-C to graphene induced by a catalytic Ni layer during annealing

Hanchao Li[a,b], Xiaowei Li[a,d], Jing Wei[a], Zhenyu Wang[a], Peng Guo[a], Peiling Ke[a,c], Hidetoshi Saito[e], Ping Cui[a,b], Aiying Wang[a,c,*]

[a] Key Laboratory of Marine Materials and Related Technologies, Zhejiang Key Laboratory of Marine Materials and Protective Technologies, Ningbo Institute of Materials Technology and Engineering, Ningbo Institute of Industrial Technology, Chinese Academy of Sciences, Ningbo 315201, China
[b] School of Physical Science and Technology, ShanghaiTech University, Shanghai 201210, China
[c] Center of Materials Science and Optoelectronics Engineering, University of Chinese Academy of Sciences, Beijing 100049, China
[d] Computational Science Center, Korea Institute of Science and Technology, Seoul 136-791, Republic of Korea
[e] Graduate School of Engineering, Nagaoka University of Technology, 1603-1 Kamitomioka-machi, Nagaoka, Niigata 940-2188, Japan

ARTICLE INFO

Keywords:
Amorphous carbon
Nickel catalyst
Graphene
Thermal annealing

ABSTRACT

As an alternative strategy to fabricate high-performance graphene over a large area, metal catalysis has been attempted at elevated temperatures with various solid carbon sources such as polymers and amorphous carbon. Due to the diversity of amorphous carbon materials and the variety of metal catalysts used in the processes, the crystalline transformation from the amorphous carbon state to the graphene phase is not yet clearly understood. Here, we fabricated hydrogen free tetrahedral amorphous carbon (ta-C) as a solid carbon source, and nickel was chosen for the catalytic metal layer, which thereafter were integrated into a designed Si/SiO_2/ta-C/Ni sandwich structure. The effect of thermal annealing in the range of 400 °C to 900 °C on the transformation of atomic carbon bonds was investigated. The results showed that the formation of the graphene phase emerged at an annealing temperature of 600 °C. Further increasing the temperature to 900 °C stimulated enhanced quality of graphene, but the quality was poor due to the oversaturated carbon content and the agglomeration of the Ni layer. Decreasing the thickness of ta-C to 2 nm led to graphene with 3–4 layers at a temperature of 800 °C, where metal-induced layer exchange was proposed as the key factor for the crystalline transformation from ta-C to graphene during thermal annealing. The results introduce a new strategy for the fabrication of high-quality graphene from tetrahedral amorphous carbon.

1. Introduction

Carbon nanostructures have a rich variety of forms including amorphous structures, such as carbon black, glassy carbon and amorphous carbon (a-C, also called diamond-like carbon) [1], and crystalline forms, such as fullerenes [2], carbon nanotubes [3], and graphene [4]. Owing to its unique structure and excellent mechanical, electronical, thermal and optical properties [5–8], graphene, fabricated by Geim for the first time through the graphite exfoliating method, has gotten more and more attention as a new material. These excellent properties make it a promising candidate for industrial applications in biological medicine [9], super capacitors [10], solar cells [11,12], high-frequency field effect transistors [13], etc.

So far, various methods have been developed to produce graphene including mechanical exfoliation [4], epitaxial growth [14,15], chemical oxidation-reduction [16,17], chemical vapor deposition (CVD) [18,19], etc. Recently, there has been research showing that graphene can be synthesized from solid carbon sources, such as polyethylene (PE), polyethylene glycol (PEG), poly (methyl methacrylate) (PMMA), polystyrene (PS), amorphous carbon, etc., via thermal annealing [20–22].

The conversion of amorphous carbon to graphene via nickel catalysis has been reported. Zheng et al. reported the synthesis of graphene using amorphous carbon via the catalysis of nickel and cobalt for the first time, pointing out the feasibility of the synthesis of graphene with amorphous carbon [23]. Xiong et al. fabricated large-area monolayer graphene at 1100 °C successfully and discussed the detailed ratio of nickel to carbon in the formation of graphene [24]. The influences of

* Corresponding author at: Key Laboratory of Marine Materials and Related Technologies, Zhejiang Key Laboratory of Marine Materials and Protective Technologies, Ningbo Institute of Materials Technology and Engineering, Ningbo Institute of Industrial Technology, Chinese Academy of Sciences, Ningbo 315201, China.
E-mail address: aywang@nimte.ac.cn (A. Wang).

https://doi.org/10.1016/j.diamond.2019.107556
Received 5 July 2019; Received in revised form 6 September 2019; Accepted 24 September 2019
Available online 19 October 2019
0925-9635/

oxygen-free environments, cooling rate and crystallinity of metal films in the formation of graphene have been investigated [25,26]. The quality of graphene synthesized from amorphous carbon is similar to that of graphene fabricated by the CVD method [27,28]. Nevertheless, detailed diffusion behavior and the transformation of amorphous carbon are rarely mentioned.

Amorphous carbon has a variety of forms [29], including hydrogen diamond-like carbon, metal doping diamond-like carbon, graphite-like carbon (glc) and tetrahedral amorphous carbon (ta-C). In previous publications [24–26], the type of amorphous carbon used to synthesize graphene has been glc fabricated by magnetron sputtering. Compared with other amorphous carbon, such as glc, ta-C possesses high sp^3 content, high hardness, high elastic modulus and dense structure [30,31]. The previous research proved that the sp^3 carbon was prone to form graphitic structure with nickel catalysis [32], and calculation results also showed that graphene was more easily transformed from high density amorphous carbon [33]. In addition, due to the convenience of ultrathin ta-C preparation, the content of solid carbon source can be controlled easily in graphene synthesis. However, the investigation of ta-C transformation in terms of experiment is lacking and related mechanism is confusing. Thus, more attention should be paid to the investigation of ta-C transformation.

In this paper, we investigated the transformation of ta-C with Ni catalyst after annealing at temperatures ranging from 400 °C to 900 °C systematically. The diffusion behavior of ta-C was discussed in detail. Graphene was formed at 600 °C. The layer exchange of nickel and ta-C occurred at 800 °C. Owing to the oversaturation of carbon, the quality of graphene was poor. High-quality graphene with few layers was fabricated at 800 °C with 2 nm ta-C. The number of graphene layers could be modulated by adjusting the initial thickness of ta-C, which optimized the controllability of graphene synthesis and reduced the complexity of experimental manipulation. Our results give insights into graphene synthesis using ta-C and elucidate the mechanism of transformation.

2. Experimental

2.1. Deposition process and annealing experiments

A single side polished Si wafer with a 300 nm-thick thermally oxidized SiO_2 layer (300 nm SiO_2/Si is referred to as the "SiO_2 wafer" in this paper) was used as the substrate and pretreated before deposition process. The SiO_2 wafer was placed in anhydrous acetone and anhydrous ethanol for 10 min, respectively. After ultrasonic cleaning, the SiO_2 wafer was placed in a homemade double bend filtered cathode vacuum arc (FCVA) device chamber, as shown in Fig. 1(a). A round high purity graphite (99.99%) with a diameter of 60 mm was used as the target material. There was a permanent magnet behind the target material and four magnetic coils (source magnetic (SM) coil, extraction magnetic (EM) coil, bending magnetic (BM) coil and output magnetic (OM) coil) around the double bend. By regulating the current of the four magnetic coils, we can realize the filtration of most liquid particles with double-bend assistance and control the motion of the plasma. Thus, uniform ultrathin ta-C films can be fabricated. When the base vacuum was pumped to below 2.0×10^{-5} Torr, ta-C films were deposited under specific parameters by filtered arc deposition. The Ar flow rate was 1.5 sccm. The arc current of the graphite target was fixed at 50 A, and the substrate bias was set to 80 V. The currents in the SM, EM, BM and OM coils were 5.0 A, 4.5 A, 4.5 A and 4.5 A, respectively. The thickness of the ta-C film was 40 nm. After ta-C deposition, nickel film with thickness of 80 nm was deposited on ta-C by direct current magnetron sputtering when the chamber pressure was evacuated to 2.0×10^{-5} Torr. The gas flow rate of Ar was 40 sccm and the power of the nickel target was 0.2 kW. The substrate bias was set to 50 V. Fig. 1(b) shows the schematic graph of magnetron sputtering of Ni. In addition, to synthesize high-quality graphene with a selected number of layers, 2 nm and 5 nm ta-C were fabricated.

After finishing the deposition process, the SiO_2 wafer/40 nm ta-C/80 nm nickel sample was placed in a quartz tube (MTI-OTF-1200X) for annealing experiments. The annealing temperature ranged from 400 °C to 900 °C in a vacuum environment, and the pressure was less than 10^{-2} Pa. The heating rate was 100 °C/min, and the thermal annealing time was 1 h. The sample cooled down to room temperature (RT) naturally.

2.2. Sample characterization

The chemical composition and bonding states were measured by X-ray photoelectron spectroscopy (XPS) using a Kratos Axis Ultra DLD instrument with a monochromic Al K_α X-ray source ($h\nu = 1486.6$ eV). The power was 96 W and the X-ray spot size was set to 700 × 300 μm. The sample was etched for 2 min under 2 kV beam energy to remove surface adsorbate. The pass energy of the XPS analyzer was set to 20 eV. The base pressure of the analysis chamber was better than 5×10^{-9} Torr. The surface morphology and structure were evaluated by scanning electron microscope (SEM, Hitachi S4800). The phase constitution of the as-deposited and annealed films was investigated by X-ray diffraction (XRD, Bruker D8 Advance) using Cu Ka radiation ($\lambda = 0.15406$ nm) scanning from 10° to 60° in the 2θ range with a 0.02° step interval and 0.2 s/step counter time. The elemental distribution was identified by energy dispersive spectroscopy (EDS, FEI Quanta FEG 250). The quality of the annealed sample was analyzed using Raman spectroscopy (Renishaw inVia Reflex) with a 532 nm excitation wavelength and 5 mW incident laser power. The depth profile analysis was carried out by glow discharge optical emission spectrometer (GDOES, Spectruma Analytik GmbH). High-resolution transmission electron microscopy (HR-TEM, FEI Tecnai F20) was employed to reveal the microstructure of the sample and analyze the element distribution. The specimens for TEM were prepared as follows. Disc shaped samples with a diameter of 3 mm and several of nanometers thickness at the center

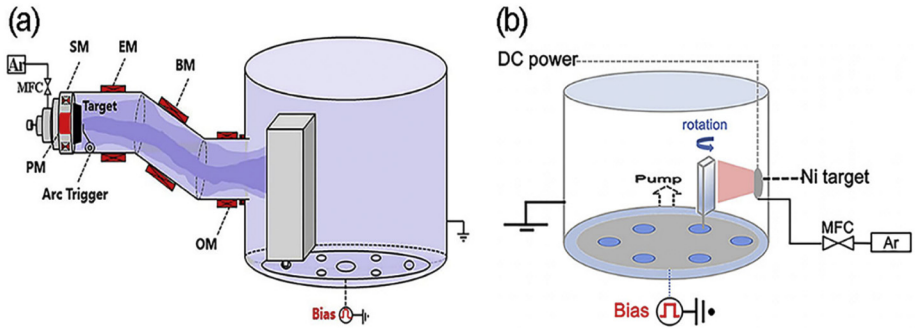

Fig. 1. (a) The schematic graph of the homemade double bend FCVA device, clearly showing the deposition of ta-C. (b) The schematic graph of nickel deposition by magnetron sputtering.

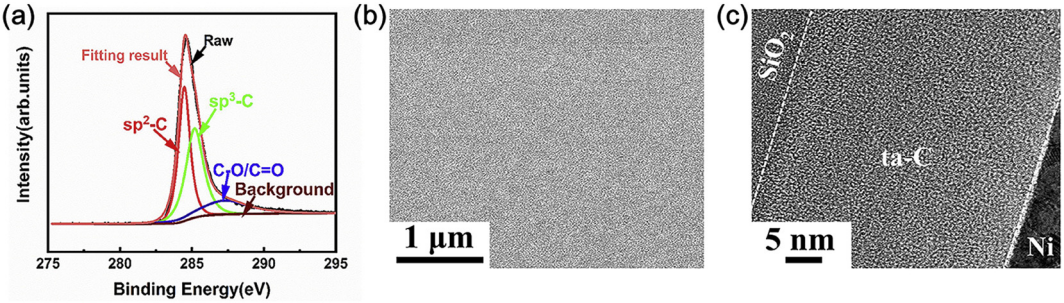

Fig. 2. (a) XPS analysis of the C1s of 40 nm ta-C. (b) The SEM image of surface morphology of the as-deposited SiO_2 wafer/40 nm ta-C/80 nm Ni sample. (c) High resolution transmission electron microscopy (HR-TEM) image of the SiO_2 wafer/40 nm ta-C/80 nm Ni.

were prepared by using the techniques of ultrasonic cutting, two-side mechanical polishing and ion beam (Ar^+) milling.

3. Results and discussion

3.1. Structural characterization of as-deposited films

To determine the sp^3 content of ta-C, XPS spectra of ta-C were measured. As shown in Fig. 2(a), the C1s peak was deconvoluted into three peaks: C=C (sp^2) approximately 284.4 ± 0.2 eV, C−C (sp^3) approximately 285.3 ± 0.2 eV, and C-O/C=O approximately 287.5 ± 0.2 eV [34,35]. The sp^3 content was approximately 52.7% according to the ratio of the area under the corresponding sp^3 distribution to the sum of the areas under the sp^2 and sp^3 distributions. As shown in Fig. 2(b), the surface morphology of SiO_2 wafer/40 nm ta-C/80 nm Ni was uniform and smooth, suggesting that nickel completely covered ta-C. The microstructure of the sample is shown in Fig. 2(c). The sandwich structure of the SiO_2 wafer/40 nm ta-C/80 nm Ni sample is easily distinguished.

3.2. Diffusion and crystallization of ta-C

Fig. 3 shows the evolution of the surface morphology of samples after annealing at different temperatures. There was no obvious difference between the as-deposited sample and samples annealed at 400 °C and 500 °C (Fig. 3(a) and (b)), indicating that the energy was too low to induce structural and morphological changes [23]. However, at 600 °C, the morphological changes could be clearly distinguished because of the changes of surface roughness (Fig. 3(c)). It was speculated that ta-C diffused into Ni surface leading to a change in morphology which intensified with increasing temperature. The morphology of the sample after annealing at 700 °C is shown in Fig. 3(d). The change in morphology was more obvious, indicating further enhanced diffusion of ta-C. Fig. 3(d-1) and (d-2) show the EDS analysis data of Fig. 3(d), representing the distribution of nickel and carbon, respectively. The results of SEM and the corresponding EDS showed that the white and gray areas were nickel-rich. As shown in Fig. 3(d–f), the black areas enlarged with increasing temperature within the range from 700 °C to 900 °C, implying that the carbon-rich areas increased. In addition, as shown in Fig. 3(e–f), the white and gray phase enlarged, implying the growth of nickel grains. It was obvious that nickel agglomerated at 900 °C because of Ostwald ripening [36], leading to the appearance of island shapes of nickel surrounded by carbon. Although carbon signals covered almost the entire surface due to the solubility of carbon in nickel, the distribution of carbon and nickel could be distinguished by the distribution of nickel. The results at 900 °C implied that excessive energy caused agglomeration of nickel [37]. However, at low temperatures, the low catalytic activity of nickel prevented the formation of graphene. Therefore, it is of great significance to fabricate graphene at an appropriate temperature.

During the annealing process, we inferred that the diffusion of carbon played a critical role which resulted in morphological changes.

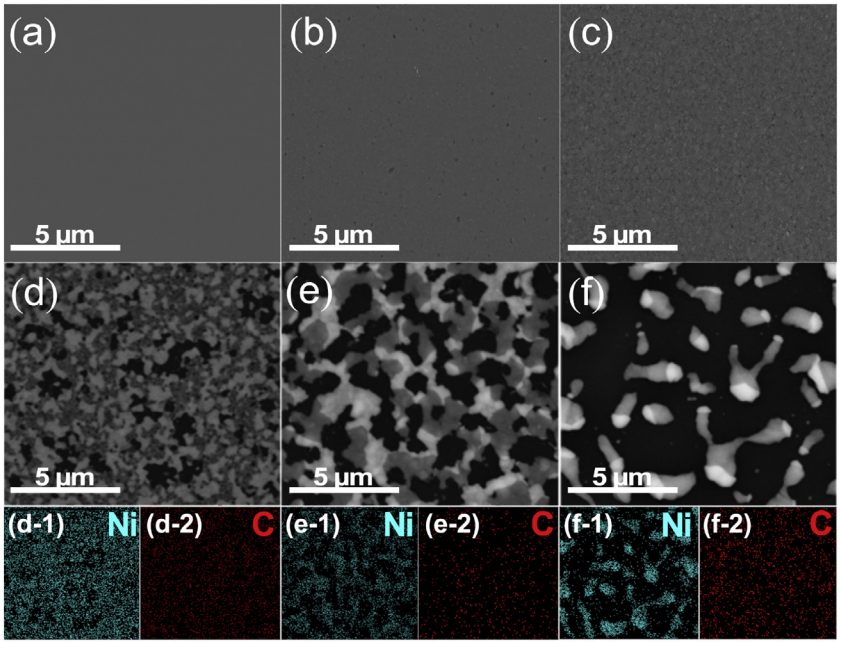

Fig. 3. SEM images of surface morphology of the SiO_2 wafer/40 nm ta-C/80 nm Ni samples after annealing at different temperatures for 1 h. (a) 400 °C. (b) 500 °C. (c) 600 °C. (d) 700 °C. (e) 800 °C. (f) 900 °C. The color images of (d-1), (e-1) and (f-1) represent the Ni distribution of (d), (e) and (f) respectively. The color images of (d-2), (e-2) and (f-2) represent the C distribution of (d), (e) and (f) respectively.

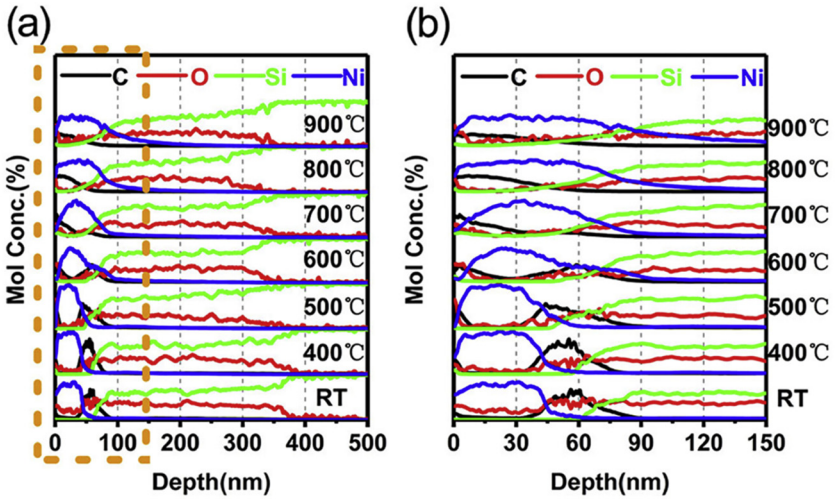

Fig. 4. (a) The depth profile of up to 500 nm of the samples after annealing at different temperatures. (b) The depth profile of samples from the surface to a 150 nm depth, which is marked with an orange rectangle in (a).

To verify that assumption and reveal the diffusion process in detail, GDOES was measured. Fig. 4(a) shows the depth profile of samples from the surface to 500 nm. Fig. 4(b), marked with an orange rectangle in Fig. 4(a), shows the depth profile from the surface to 150 nm of the samples. At room temperature (RT), it could be clearly seen that ta-C was in the middle layer between nickel and SiO_2. There was no obvious change when sample was annealed at 400 °C, indicating no diffusion behavior of carbon. Wenisch et al. pointed out that surface diffusion overwhelmed bulk diffusion at low temperatures (550 °C) [38]. However, at 500 °C, the carbon distribution curve in Fig. 4(b) slightly changed since the peak of carbon shifted towards the surface, indicating carbon bulk diffusion had begun. Compared with surface diffusion, bulk diffusion reached a comparable level at 500 °C. In addition, there was no carbon signal in the subsurface ranging from the surface to a depth of 10 nm suggesting that the signal of carbon on the surface was caused by absorbed substance. As shown in Fig. 4(b), carbon obviously diffused to the surface at 600 °C. The peak value of carbon in the middle layer obviously dropped and the carbon signal appeared on the surface. Additionally, the broad C peak ranging from 45 nm to 75 nm in Fig. 4(b) shows that the bulk carbon reservoir was adequate, indicating that just a portion of carbon diffused to surface. There was still carbon in the inner layer. Compared to the result at 600 °C, the result at 700 °C showed that most carbon diffused to the surface, leading to a dramatic change in depth profile with a slope shape from the surface to bulk phase. At 800 °C, carbon and nickel underwent a dramatic change. The nickel peak obviously shifted towards the substrates demonstrating that nickel diffused to the SiO_2 interface. The carbon signal was almost undetectable from 45 nm to 100 nm indicating that there was no carbon residue in the middle layer. Thus, ta-C had permeated through nickel and precipitated on nickel surface. Compared with the result at 800 °C, the result at 900 °C showed no dramatic change in the carbon depth profile. The result showed that carbon permeated through nickel completely, which is similar to a previous research [39].

Meanwhile, after the annealing process, the sample might undergo conversion due to graphitization of ta-C via nickel catalysis [23–25], which cannot be easily distinguished by SEM and GDOES. Thus, Raman spectra were employed to reveal the structural conversion as seen in Fig. 5(a). The as-deposited sample showed no obvious peak. With increasing temperature, ta-C dissolved into nickel and then precipitated on the surface. However, at low temperatures (400 °C, 500 °C), the D peak (~1350 cm^{-1}) and G peak (~1590 cm^{-1}) were difficult to detect, showing that very little ta-C diffused to the surface due to the lack of energy [40]. The D peak (~1350 cm^{-1}) indicated the disorder in the graphite layer and the G peak (~1590 cm^{-1}) was the characteristic peak of the sp^2 structure of carbon [41]. At 600 °C, ta-C could not only diffuse to the surface but also could transform into a crystal structure. Unfortunately, the broad D peak and G peak in Raman spectroscopy demonstrated that the catalytic activity of nickel was inadequate. The signal from the 2D peak (~2690 cm^{-1}), a typical feature of graphene, indicated that the conversion of ta-C occurred [23,41]. With temperature increasing from 700 °C to 900 °C, the intensity of the 2D peak was enhanced, showing that the crystallization of ta-C increased due to strong nickel catalysis [23].

The orientation of nickel plays a significant role in the formation of graphene, which has been discussed in previous literatures [42–44]. Different nickel crystal planes have different surface potential energies, which affects the process of precipitation and the crystallization of carbon. Ni (111) has a better lattice match for the growth of graphene [44]. As shown in Fig. 5(b), the peak at 44.5° showed that the nickel in the as-deposited sample displayed the Ni (111) orientation. After annealing at low temperatures under 600 °C, only the diffraction peak of Ni (111) appeared. When the annealing temperature was above 600 °C, diffraction peaks at 26.6° and 51.9° appeared, corresponding to graphite (002) and Ni (200), respectively [45,46]. As the annealing temperature increased from 700 °C to 900 °C, the measurable graphite (002) peak confirmed the formation of multilayer graphene. The intensity of Ni (111) and Ni (200) enhanced, suggesting nickel grains were growing significantly. The appearance of Ni (200) affected the quality of graphene because of the lattice mismatch. The intensity of graphite (002) weakened slightly, suggesting that the growth of nickel was dominant in this process from 700 °C to 900 °C. The above results showed that graphitization of ta-C occurred above 600 °C. However, the microstructural evolution of the sample was unclear. Thus, the microstructure should be investigated in detail to confirm the conversion and reveal the formation mechanism of graphene.

Transmission electron microscopy (TEM) was employed to reveal the evolution of microstructure. As shown in Fig. 6(a), the TEM images of the sample after annealing at 400 °C displayed a visible sandwich structure for SiO_2/ta-C/Ni. There was no carbon on the surface of nickel, demonstrating that the energy for carbon bulk diffusion was insufficient [38]. There was almost no difference between the as-deposited sample and the sample annealed at 400 °C. Fig. 6(b) and (c) show the Ni/C interface and C/SiO_2 interface, respectively. Only the Ni/C interface yielded a small layer structure with few (2–6) graphitic carbon planes parallel to the Ni/C interface which are marked with a red circle with a dashed line. Owing to poor nickel catalysis, only a small part of ta-C transformed, and that occurred at the C/Ni interface. At the same time, the structure and morphology of the C/SiO_2 interface

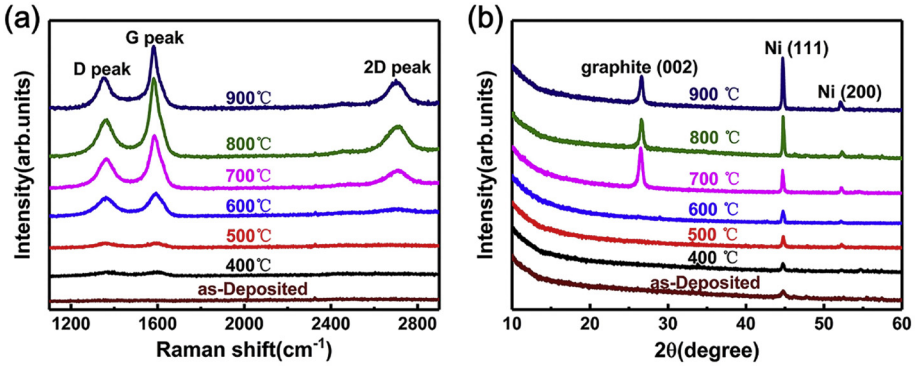

Fig. 5. (a) Raman spectra of the SiO_2 wafer/40 nm ta-C/80 nm Ni samples after annealing at different temperatures for 1 h. (b) Corresponding XRD data of samples after annealing at different temperatures for 1 h.

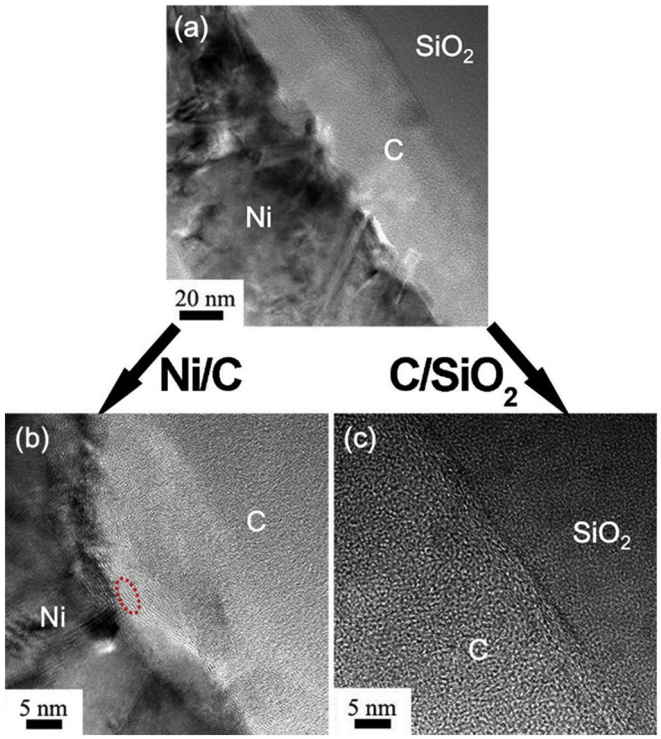

Fig. 6. TEM images of the SiO_2 wafer/40 nm ta-C/80 nm Ni sample after annealing at 400 °C for 1 h. (a) Low magnification TEM image of SiO_2/ta-C/Ni clearly shows a sandwich structure. (b) HR-TEM image of the Ni/C interface. The red circle shows the sp^2 cluster, demonstrating the graphitization of some ta-C at the Ni/C interface. (c) Compared to the as-deposited sample, HR-TEM image of the C/SiO_2 interface after annealing at 400 °C shows no obvious difference. (For interpretation of the references to color in this figure legend, the reader is referred to the web version of this article.)

remained unchanged.

However, there was an obvious change after the sample was annealed at 500 °C, as shown in Fig. 7(a). The carbon layer moved slightly towards the surface at 500 °C forming a Ni/C/Ni sandwich structure owing to its solubility in nickel [27]. Fig. 7(b) shows the high-angle annular dark-field (HAADF)-STEM graph of area marked with a red rectangle in Fig. 7(a). According to the element distribution map (Fig. 7(b)), the results suggested that the diffusion of ta-C towards the surface led to the substitution of the Ni/SiO_2 interface for the original C/SiO_2 interface. Moreover, as shown in Fig. 7(c), there was no carbon remaining at the Ni/SiO_2 interface, which is inconsistent with the dissolution-precipitation mechanism [27]. As shown in Fig. 7(c), the appearance of onion-carbon which was circled by a dotted red line indicated that the graphitization of ta-C occurred [40]. Owing to an atomic level coherent match between nickel and graphite, graphene was parallel to nickel in Fig. 7(d). The orientation of graphene away from the C/Ni interface was randomly arranged, which indicated that the quality and controllability of graphene were poor [38]. In addition, the amorphous structure of carbon still existed, indicating that the catalytic capacity of nickel was insufficient [46]. On the sample surface, there was no carbon, indicating that carbon in the middle layer lacked the ability to diffuse further.

The microstructure of samples after annealing at 600 °C, 700 °C and 800 °C is shown in Fig. 8, and the structure changed from SiO_2/Ni/C/Ni to SiO_2/Ni/C/Ni/graphene. A portion of ta-C diffused to the surface and formed graphene at 600 °C, as shown in Fig. 8(a) and (b), indicating the feasibility of graphene synthesis at low temperature [47]. However, the quality of graphene still should be improved because of inadequate nickel catalysis [23]. Although the ability of carbon to diffuse increased with rising temperature, there was still no carbon residue at the Ni/SiO_2 interface after annealing process as shown in Fig. 8(c). At 700 °C, the content of graphene on the surface increased further, forming multilayer graphene as shown in Fig. 8(d). As shown in Fig. 8(e), the graphene was more homogeneous and smoother than the result which formed at 600 °C. Meanwhile, there was still carbon in the bulk of the sample and no carbon at the Ni/SiO_2 interface as shown in Fig. 8(f). At 800 °C, it showed that carbon permeated through the nickel layer and graphene formed on the surface, as shown in Fig. 8(g). All carbon diffused to the surface, leading to an absence of carbon residue at the Ni/SiO_2 interface (Fig. 8(i)). That indicated the mechanism was not simple dissolution-precipitation, which could not account for the previous observation. According to our findings, results could be explained by a metal-induced layer exchange [39,48].

As shown in Fig. 9(a), the agglomeration of nickel occurred after the sample was annealed at 900 °C [37]. At this time, graphene was connected to two isolated Ni particles (Fig. 9(b)). Unfortunately, the graphene was damaged to a certain degree by the agglomeration of nickel, as shown in Fig. 9(c). Because 900 °C was not conducive to the synthesis of high-quality graphene, it may be appropriate to produce graphene at 800 °C to avoid the agglomeration of nickel.

3.3. The transformation mechanism of ta-C to graphene

For graphene synthesis via nickel catalysis, the dissolution-precipitation mechanism has been reported in previous research paper [27]. In this process, carbon dissolves in nickel metal while temperature increases, and upon cooling graphene is believed to precipitate from the dissolved carbon atoms in nickel [44]. Another mechanism for graphene synthesis is metal induced crystallization, which was proposed by Saenger et al. owing to the detected signal of graphite (002) peak by in situ XRD during the heating process [45]. Wenisch et al. believe the formation of graphitic carbon is due to surface diffusion-assisted

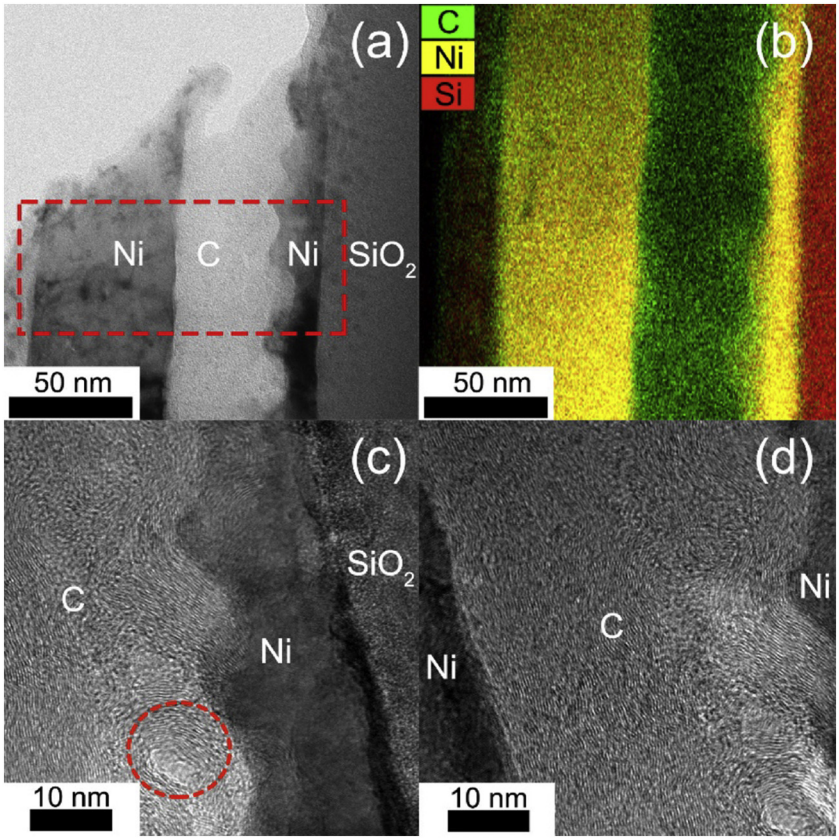

Fig. 7. (a) Low magnification TEM image of the SiO_2 wafer/40 nm ta-C/80 nm Ni after annealing at 500 °C. (b) HADDF image shows the corresponding element distribution of the part marked with a red rectangle in (a), which clearly shows the Ni/C/Ni sandwich structure. (c) The inner microstructure of the SiO_2 wafer/Ni/C. The onion-carbon is marked by a red dotted circle. (d) HR-TEM image of the Ni/C/Ni sandwich structure. (For interpretation of the references to color in this figure legend, the reader is referred to the web version of this article.)

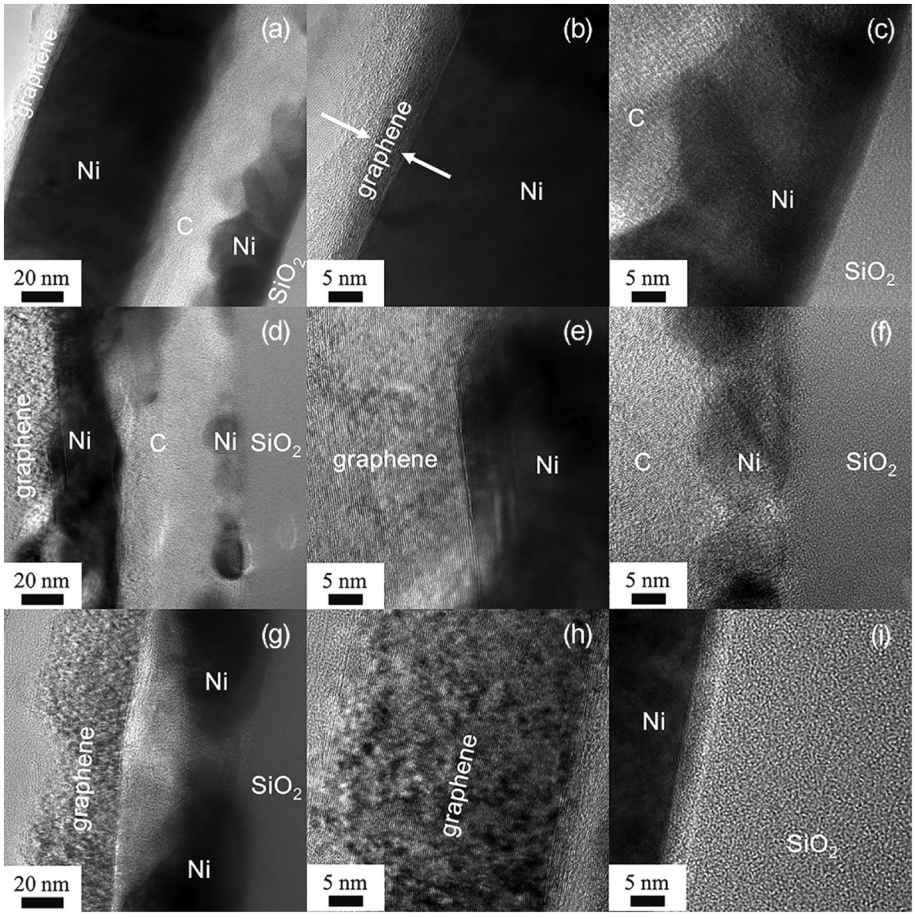

Fig. 8. (a), (d) and (g) show low magnification TEM images of the samples after annealing at 600 °C, 700 °C and 800 °C, respectively. (b), (e) and (h) show corresponding HR-TEM images of surface graphene in (a), (d) and (g) respectively. (c), (f) and (i) show corresponding HR-TEM images of the Ni/SiO_2 microstructure in (a), (d) and (g) respectively.

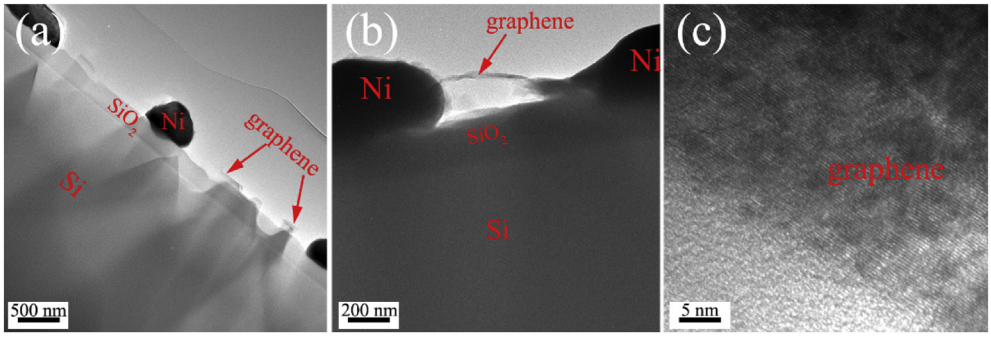

Fig. 9. (a) Low magnification TEM image of the sample after annealing at 900 °C. (b) Two Ni particles were connected by graphene. (c) HR-TEM image of graphene which was destroyed by the agglomeration of nickel.

crystallization [38].

However, some phenomena in this paper cannot be reasonably explained by these mechanisms. Owing to the absence of graphene or carbon residue at the Ni/SiO_2 interface in our TEM results, the dissolution-precipitation mechanism was ruled out. Surface diffusion-assisted crystallization cannot account for experimental results because of obvious carbon diffusion towards the surface. It is worth mentioning that the formation of the sp^2 cluster at the interface and the onion-carbon formation can be explained by this mechanism. Furthermore, surface diffusion-assisted crystallization can only account for graphitization at a low temperature (< 500 °C), indicating this mechanism cannot account for experimental results when temperature is above 500 °C. Because carbon permeated through the nickel layer and the conversion of ta-C occurred, the metal-induced layer exchange mechanism is acceptable, which is similar to Al-induced Si crystallization and layer exchange [48]. In addition, layer exchange occurred at an appropriate temperature, as ta-C diffused through nickel and produced graphene. In our experiments, 800 °C was found to be the appropriate temperature for thermal annealing.

Fig. 10 shows the schematic graph of the graphene growth mechanism. Carbon diffused towards the surface due to its solubility in nickel as temperature increased. Meanwhile, the position of the original ta-C layer was replaced by nickel, indicating layer exchange between carbon and nickel occurred. At a low temperature (500 °C), the carbon diffused into bulk nickel forming the SiO_2 wafer/Ni/amorphous and crystalline carbon/Ni structure. Crystallization of ta-C was due to metal-induced graphitization [38,45], forming a graphene nanosheet in parallel with the surface of nickel, which occurred only at the C/Ni interface. However, due to insufficient nickel catalysis at low temperature, large-area and high-quality graphene could still not be produced and most of the carbon was still amorphous. In addition, the layer exchange between carbon and nickel occurred incompletely and just formed the Ni/C/Ni sandwich structure. With the temperature increasing further (at 600 °C and 700 °C), a portion of carbon diffused to the surface and formed graphene while some was still in the bulk, indicating that the diffusion behavior of carbon was not a complete layer movement. Instead, the diffusion process happened layer by layer, indicating that high-quality graphene could be formed in a controlled way at the appropriate temperature when the layer exchange occurred. At 800 °C, layer exchange occurred, and graphene was formed on the surface of nickel. It was not advisable to increase the annealing temperature after layer exchange completely occurred. There was no carbon residue at the Ni/SiO_2 interface over the whole range of temperatures, showing that graphene formation occurred via the metal-induced layer exchange mechanism [48], rather than the simple dissolution-precipitation mechanism [27].

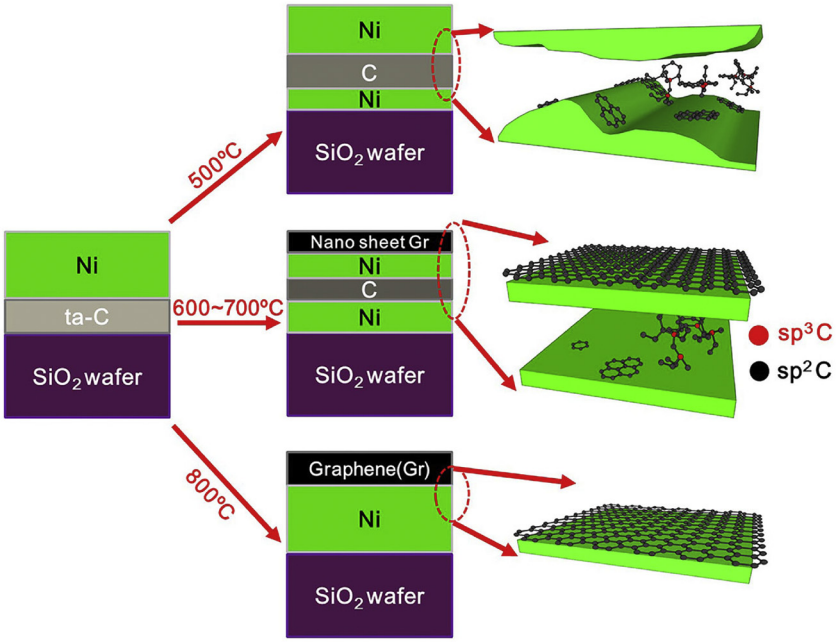

Fig. 10. The schematic graph of metal-induced layer exchange mechanism and growth process of graphene.

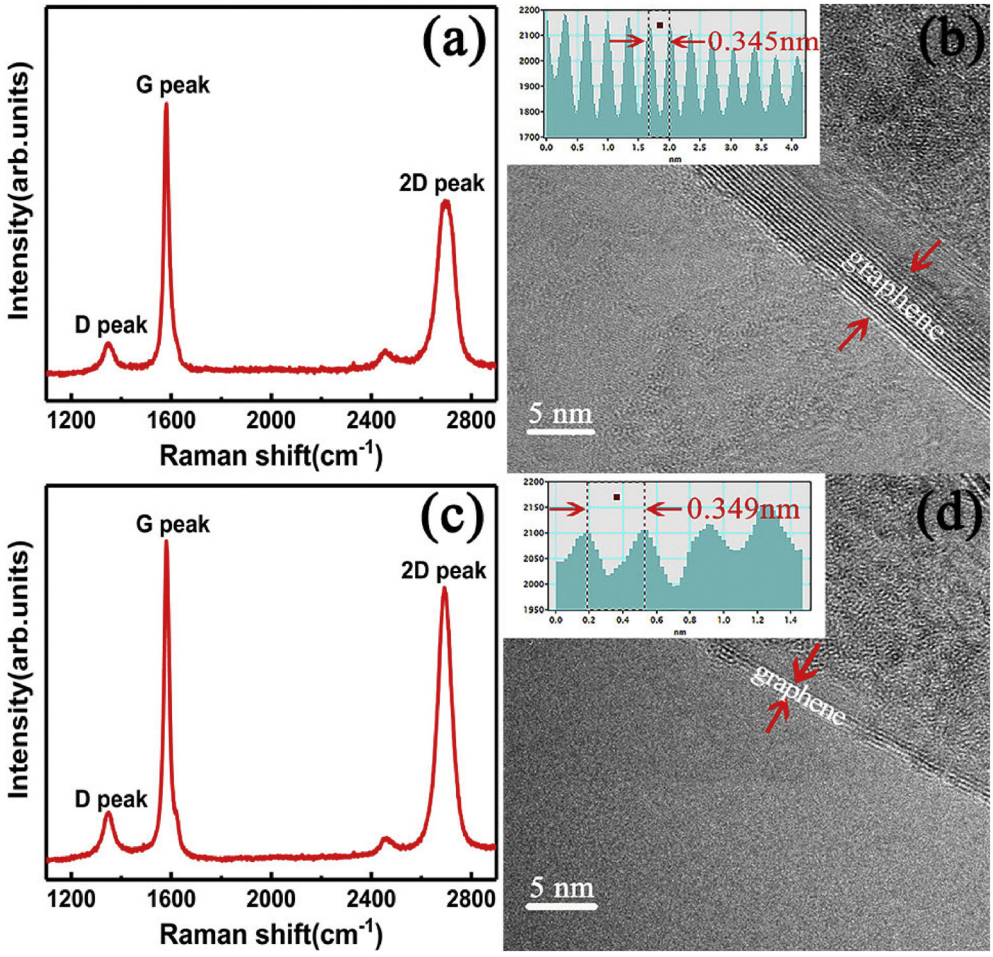

Fig. 11. (a) Raman spectra of the growth of multilayer graphene which was synthesized from 5 nm ta-C. (b) Corresponding HR-TEM image of (a). (c) Raman spectra of the growth of a few layers of graphene synthesized from 2 nm ta-C. (d) Corresponding HR-TEM image of (c).

3.4. High-quality and controllable synthesis of graphene

According to our findings, the annealing temperature and thickness of ta-C are key factors in the synthesis of high-quality graphene. Thus, 2 nm and 5 nm ta-C were fabricated. Then, 80 nm nickel was deposited, and the sample was annealed at 800 °C for 1 h. Fig. 11(a) shows the Raman spectra of the SiO_2 wafer/5 nm ta-C/80 nm Ni sample after annealing. The ratio of the D peak intensity to the G peak intensity (I_D/I_G) was 0.12, which demonstrated that graphene had a few defects. The ratio of the 2D peak intensity to the G peak intensity (I_{2D}/I_G) was less than 0.6, indicating the formation of multilayer graphene. Fig. 11(b) displays the TEM image of transferred graphene on a Cu grid, showing approximately 12 layers. Fig. 11(c) shows the Raman spectra of the SiO_2 wafer/ta-C (2 nm)/Ni sample after annealing. The I_{2D}/I_G was 0.86, which shows approximately tri-layer graphene [24]. The I_D/I_G was 0.12, demonstrating that the quality of the graphene was good. The TEM image shows three to four graphene layers in Fig. 11(d); these data, combined with the Raman spectra, indicate that the number of graphene layers is dependent on the initial thickness of ta-C.

Fig. 12 shows the mapping image of Raman spectra of SiO_2 wafer/2 nm ta-C/80 nm Ni sample after annealing at 800 °C. The ratio of I_D/I_G was shown in Fig. 12(a) and the ratio of I_{2D}/I_G was shown in Fig. 12(b), representing the quality of graphene and the numbers of graphene layers, respectively. The ratio of I_D/I_G was approximately 0.3, demonstrating the quality was well. The ratio of I_{2D}/I_G in the mapping image was almost above 1, indicating the formation of bilayer graphene and uniformness of graphene [24].

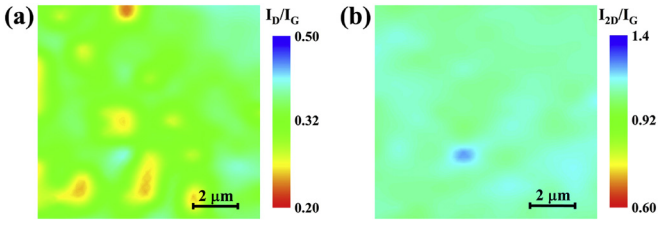

Fig. 12. The Raman spectra mapping image of SiO_2 wafer/2 nm ta-C/80 nm Ni after annealing at 800 °C for 1 h. (a) The ratio of I_D/I_G (b) The ratio of I_{2D}/I_G.

4. Conclusion

In this study, we investigated the carbon diffusion and growth process of graphene, which supported the metal-induced layer exchange mechanism rather than the simple dissolution-precipitation mechanism. Controlled production of high-quality graphene with a selected number of layers in a large quantity is dependent on the growth temperature and thickness of ta-C. The conversion of ta-C can occur at low temperature (500 °C) with nickel catalyst. However, layer exchange between nickel and ta-C occurred completely only at 800 °C. Over 800 °C, agglomeration of nickel occurred, which affected the quality of graphene. Our experiments give insights into the growth mechanism of graphene synthesized from a solid carbon source. In addition, the results indicate that the number of graphene layers is dependent on the initial thickness of ta-C.

Declaration of competing interest

The authors declare that they have no conflicts of interest to this work.

Acknowledgements

The authors thank the help of Chen Ye for the sample preparation for TEM. This research was financially supported by the A-class pilot of the Chinese Academy of Sciences (XDA22010303), National Science and Technology Major Project (2017-VII-0012-0108), the Ningbo Science and Technology Innovation Project (2018B10014), and the Major Science and Technology Project of Jiangbei District, Ningbo (201801A03).

References

[1] S. Aisenberg, R. Chabot, Ion-beam deposition of thin films of diamondlike carbon, J. Appl. Phys. 42 (7) (1971) 2953–2958.
[2] H. Kroto, J. Heath, S. O'Brien, R. Curl, R. Smalley, C60: buckminsterfullerene, Nature 318 (1985) 162–163.
[3] S. Iijima, Helical microtubules of graphitic carbon, Nature 354 (1991) 56–58.
[4] K.S. Novoselov, A.K. Geim, S.V. Morozov, D. Jiang, Y. Zhang, S.V. Dubonos, I.V. Grigorieva, A.A. Firsov, Electric field effect in atomically thin carbon films, Science 306 (2004) 666–669.
[5] C. Lee, X. Wei, J.W. Kysar, J. Hone, Measurement of the elastic properties and intrinsic strength of monolayer graphene, Science 321 (5887) (2008) 385–388.
[6] S.V. Morozov, K.S. Novoselov, M.I. Katsnelson, F. Schedin, D.C. Elias, J.A. Jaszczak, A.K. Geim, Giant intrinsic carrier mobilities in graphene and its bilayer, Phys. Rev. Lett. 100 (1) (2008) 016602.
[7] A.A. Balandin, S. Ghosh, W.Z. Bao, I. Calizo, D. Teweldebrhan, F. Miao, C.N. Lau, Superior thermal conductivity of single-layer graphene, Nano Lett. 8 (3) (2008) 902–907.
[8] R.R. Nair, P. Blake, A.N. Grigorenko, K.S. Novoselov, T.J. Booth, T. Stauber, N.M.R. Peres, A.K. Geim, Fine structure constant defines visual transparency of graphene, Science 320 (5881) (2008) 1308.
[9] Y. Ohno, K. Maehashi, Y. Yamashiro, K. Matsumoto, Electrolyte-gated graphene field-effect transistors for detecting pH and protein ad-sorption, Nano Lett. 9 (9) (2009) 3318–3322.
[10] P. Yadav, A. Banerjee, S. Unni, J. Jog, S. Kurungot, S. Ogale, A 3D hexaporous carbon assembled from single-layer graphene as high performance supercapacitor, Chemsuschem 5 (11) (2012) 2159–2164.
[11] S.-S. Li, K.-H. Tu, C.-C. Lin, C.-W. Chen, M. Chhowalla, Solution-processable graphene oxide as an efficient hole transport layer in polymer solar cells, ACS Nano 4 (6) (2010) 3169–3174.
[12] M.P. Ramuz, M. Vosgueritchian, P. Wei, C.-G. Wang, Y.-l. Gao, Y.-P. Wu, Y.-S. Chen, Z.-N. Bao, Evaluation of solution-processable carbon-based electrodes for all-carbon solar cells, ACS Nano 6 (11) (2012) 10384–10395.
[13] Y.M. Lin, C. Dimitrakopoulos, K.A. Jenkins, D.B. Farmer, H.Y. Chiu, A. Grill, P. Avouris, 100-GHz transistors from wafer-scale epitaxial graphene, Science 327 (5966) (2010) 662.
[14] K.V. Emtsev, A. Bostwick, K. Horn, J. Jobst, G.L. Kellogg, L. Ley, J.L. McChesney, T. Ohta, S.A. Reshanov, J. Rohrl, E. Rotenberg, A.K. Schmid, D. Waldmann, H.B. Weber, T. Seyller, Towards wafer-size graphene layers by atmospheric pressure graphitization of silicon carbide, Nat. Mater. 8 (3) (2009) 203–207.
[15] J.H. Warner, F. Schaffel, M. Rummeli, A. Bachmatiuk, Graphene: Fundamentals and Emergent Applications, Newnes, Boston, 2012, pp. 204–213.
[16] S. Park, R.S. Ruoff, Chemical methods for the production of graphenes, Nat. Nanotechnol. 4 (4) (2009) 217–224.
[17] S. Stankovich, D.A. Dikin, R.D. Piner, K.A. Kohlhaas, A. Kleinhammes, Y. Jia, Y. Wu, S.T. Nguyen, R.S. Ruoff, Synthesis of graphene-based nanosheets via chemical reduction of exfoliated graphite oxide, Carbon 45 (7) (2007) 1558–1565.
[18] X.S. Li, W.W. Cai, J. An, S. Kim, J. Nah, D.X. Yang, R. Piner, A. Velamakanni, I. Jung, E. Tutuc, S.K. Banerjee, L. Colombo, R.S. Ruoff, Large-area synthesis of high-quality and uniform graphene films on copper foils, Science 324 (5932) (2009) 1312–1314.
[19] J. Kang, D. Shin, S. Bae, B.H. Hong, Graphene transfer: key for applications, Nanoscale 4 (18) (2012) 5527.
[20] I.I. Kondrashov, M.G. Rybin, E.A. Obraztsova, E.D. Obraztsova, Controlled graphene synthesis from solid carbon sources, Phys. Status Solidi B 256 (9) (2019) 1800688.
[21] J. Baek, M. Lee, J. Kim, J. Lee, S. Jeon, Transfer-free growth of polymer-derived graphene on dielectric substrate from mobile hot-wire-assisted dual heating system, Carbon 127 (2018) 41–46.
[22] X. Ye, H. Zhou, I. Levchenko, K. Bazaka, S. Xu, S. Xiao, Low-temperature synthesis of graphene by ICP-assisted amorphous carbon sputtering, Chem. Sel. 3 (30) (2018) 8779–8785.
[23] M. Zheng, K. Takei, B. Hsia, H. Fang, X. Zhang, N. Ferralis, H. Ko, Y.-L. Chueh, Y. Zhang, R. Maboudian, A. Javey, Metal-catalyzed crystallization of amorphous carbon to graphene, Appl. Phys. Lett. 96 (6) (2010) 063110.
[24] W. Xiong, Y.S. Zhou, L.J. Jiang, A. Sarkar, M. Mahjouri-Samani, Z.Q. Xie, Y. Gao, N.J. Ianno, L. Jiang, Y.F. Lu, Single-step formation of graphene on dielectric surfaces, Adv. Mater. 25 (4) (2013) 630–634.
[25] B.-S. Nguyen, J.-F. Lin, D.-C. Perng, Non-vacuum growth of graphene films using solid carbon source, Appl. Phys. Lett. 106 (22) (2015) 221604.
[26] C.M. Orofeo, H. Ago, B. Hu, M. Tsuji, Synthesis of large area, homogeneous, single layer graphene films by annealing amorphous carbon on Co and Ni, Nano Res. 4 (6) (2011) 531–540.
[27] X. Li, W. Cai, L. Colombo, R.S. Ruoff, Evolution of graphene growth on Ni and Cu by carbon isotope labeling, Nano Lett. 9 (12) (2009) 4268–4272.
[28] M.G. Rybin, I.I. Kondrashov, A.S. Pozharov, V.C. Nguyen, N.M. Phan, E.D. Obraztsova, In situ control of CVD synthesis of graphene film on nickel foil, Phys. Status Solidi B 255 (1) (2018) 1700414.
[29] J. Robertson, Diamond-like amorphous carbon, Mater. Sci. Eng. R 37 (4) (2002) 129–281.
[30] N. Wang, K. Komvopoulos, The multilayered structure of ultrathin amorphous carbon films synthesized by filtered cathodic vacuum arc deposition, J. Mater. Res. 28 (16) (2013) 2124–2131.
[31] J. Xie, K. Komvopoulos, Bilayer amorphous carbon films synthesized by filtered cathodic vacuum arc deposition, J. Mater. Res. 31 (20) (2016) 3161–3167.
[32] S. Chen, W. Xiong, Y.S. Zhou, Y.F. Lu, X.C. Zeng, An ab initio study of the nickel-catalyzed transformation of amorphous carbon into graphene in rapid thermal processing, Nanoscale 8 (18) (2016) 9746–9755.
[33] X. Li, Y. Zhou, X. Xu, A. Wang, K.R. Lee, Role of the carbon source in the transformation of amorphous carbon to graphene during rapid thermal processing, Phys. Chem. Chem. Phys. 21 (18) (2019) 9384–9390.
[34] G.J. Kovács, I. Bertóti, G. Radnóczi, X-ray photoelectron spectroscopic study of magnetron sputtered carbon–nickel composite films, Thin Solid Films 516 (21) (2008) 7942–7946.
[35] R.S. Weatherup, B.C. Bayer, R. Blume, C. Ducati, C. Baehtz, R. Schlogl, S. Hofmann, In situ characterization of alloy catalysts for low-temperature graphene growth, Nano Lett. 11 (10) (2011) 4154–4160.
[36] P.W. Voorhees, The theory of Ostwald ripening, J. Stat. Phys. 38 (1–2) (1985) 231–252.
[37] M. Miyoshi, M. Mizuno, K. Banno, T. Kubo, T. Egawa, T. Soga, Study on transfer-free graphene synthesis process utilizing spontaneous agglomeration of catalytic Ni and Co metals, Mater. Res. Express. 2 (1) (2015) 015602.
[38] R. Wenisch, R. Hübner, F. Munnik, S. Melkhanova, S. Gemming, G. Abrasonis, M. Krause, Nickel-enhanced graphitic ordering of carbon ad-atoms during physical vapor deposition, Carbon 100 (2016) 656–663.
[39] H. Murata, K. Toko, N. Saitoh, N. Yoshizawa, T. Suemasu, Direct synthesis of multilayer graphene on an insulator by Ni-induced layer exchange growth of amorphous carbon, Appl. Phys. Lett. 110 (3) (2017) 033108.
[40] R. Anton, On the reaction kinetics of Ni with amorphous carbon, Carbon 46 (4) (2008) 656–662.
[41] A.C. Ferrari, J.C. Meyer, V. Scardaci, C. Casiraghi, M. Lazzeri, F. Mauri, S. Piscanec, D. Jiang, K.S. Novoselov, S. Roth, A.K. Geim, Raman spectrum of graphene and graphene layers, Phys. Rev. Lett. 97 (18) (2006) 187401.
[42] J. Hofrichter, B.N. Szafranek, M. Otto, T.J. Echtermeyer, M. Baus, A. Majerus, V. Geringer, M. Ramsteiner, H. Kurz, Synthesis of graphene on silicon dioxide by a solid carbon source, Nano Lett. 10 (1) (2010) 36–42.
[43] A. Dahal, M. Batzill, Graphene-nickel interfaces: a review, Nanoscale 6 (5) (2014) 2548–2562.
[44] C.-M. Seah, S.-P. Chai, A.R. Mohamed, Mechanisms of graphene growth by chemical vapour deposition on transition metals, Carbon 70 (2014) 1–21.
[45] K.L. Saenger, J.C. Tsang, A.A. Bol, J.O. Chu, A. Grill, C. Lavoie, In situ x-ray diffraction study of graphitic carbon formed during heating and cooling of amorphous-C/Ni bilayers, Appl. Phys. Lett. 96 (15) (2010) 153105.
[46] G. Pan, B. Li, M. Heath, D. Horsell, M.L. Wears, L. Al Taan, S. Awan, Transfer-free growth of graphene on SiO_2 insulator substrate from sputtered carbon and nickel films, Carbon 65 (2013) 349–358.
[47] G. Gutierrez, F. Le Normand, D. Muller, F. Aweke, C. Speisser, F. Antoni, Y. Le Gall, C.S. Lee, C.S. Cojocaru, Multi-layer graphene obtained by high temperature carbon implantation into nickel films, Carbon 66 (2014) 1–10.
[48] J.Y. Wang, Z.M. Wang, E.J. Mittemeijer, Mechanism of aluminum-induced layer exchange upon low-temperature annealing of amorphous Si-polycrystalline Al bilayers, J. Appl. Phys. 102 (11) (2007).